



Sulfur isotope fractionation during heterogeneous oxidation of SO₂ on mineral dust

E. Harris¹, B. Sinha^{1,2}, S. Foley³, J. N. Crowley⁴, S. Borrmann¹, and P. Hoppe¹

¹Abteilung Partikelchemie, Max-Planck-Institut für Chemie, Hahn-Meitner-Weg 1, 55128 Mainz, Germany

²Department of Earth Sciences, Indian Institute for Science Education and Research IISER Mohali, Sector 81, SAS Nagar, Manauli P.O. 140306, India

³Earth System Science Research Centre, Institute for Geosciences, University of Mainz, Becherweg 21, 55128 Mainz, Germany

⁴Abteilung Luftchemie, Max-Planck-Institut für Chemie, Hahn-Meitner-Weg 1, 55128 Mainz, Germany

Correspondence to: B. Sinha (baerbel.sinha@mpic.de)

Received: 9 January 2012 – Published in Atmos. Chem. Phys. Discuss.: 25 January 2012

Revised: 7 May 2012 – Accepted: 9 May 2012 – Published: 4 June 2012

Abstract. Mineral dust is a major fraction of global atmospheric aerosol, and the oxidation of SO₂ on mineral dust has implications for cloud formation, climate and the sulfur cycle. Stable sulfur isotopes can be used to understand the different oxidation processes occurring on mineral dust. This study presents measurements of the ³⁴S/³²S fractionation factor α_{34} for oxidation of SO₂ on mineral dust surfaces and in the aqueous phase in mineral dust leachate. Sahara dust, which accounts for ~60 % of global dust emissions and loading, was used for the experiments.

The fractionation factor for aqueous oxidation in dust leachate is $\alpha_{\text{leachate}} = 0.9917 \pm 0.0046$, which is in agreement with previous measurements of aqueous SO₂ oxidation by iron solutions. This fractionation factor is representative of a radical chain reaction oxidation pathway initiated by transition metal ions. Oxidation on the dust surface at subsaturated relative humidity (RH) had an overall fractionation factor of $\alpha_{\text{het}} = 1.0096 \pm 0.0036$ and was found to be almost an order of magnitude faster when the dust was simultaneously exposed to ozone, light and RH of ~40 %. However, the presence of ozone, light and humidity did not influence isotope fractionation during oxidation on dust surfaces at subsaturated relative humidity. All the investigated reactions showed mass-dependent fractionation of ³³S relative to ³⁴S.

A positive matrix factorization model was used to investigate surface oxidation on the different components of dust. Ilmenite, rutile and iron oxide were found to be the most reactive components, accounting for 85 % of sulfate produc-

tion with a fractionation factor of $\alpha_{34} = 1.012 \pm 0.010$. This overlaps within the analytical uncertainty with the fractionation of other major atmospheric oxidation pathways such as the oxidation of SO₂ by H₂O₂ and O₃ in the aqueous phase and OH in the gas phase. Clay minerals accounted for roughly 12 % of the sulfate production, and oxidation on clay minerals resulted in a very distinct fractionation factor of $\alpha_{34} = 1.085 \pm 0.013$. The fractionation factors measured in this study will be particularly useful in combination with field and modelling studies to understand the role of surface oxidation on clay minerals and aqueous oxidation by mineral dust and its leachate in global and regional sulfur cycles.

1 Introduction

Mineral dust represents the dominant mass fraction of atmospheric particulate matter, and it is responsible for a large amount of the uncertainty associated with aerosol climate forcing effects. Dust is important for heterogeneous chemistry, human health, visibility, ocean nutrification, and cloud formation. Mineral dust emissions are estimated to be between 1000 and 2150 Tg yr⁻¹, resulting in a global dust load of 8 to 36 Tg (Zender et al., 2004; Tanaka and Chiba, 2006). Dust emissions are expected to increase due to erosion, mining and industrial activities, overgrazing and shifting precipitation patterns (Dentener et al., 1996). Mineral dust properties are altered during transport, as finer clays are transported

far from source regions relative to coarse particles, and dust particles are chemically aged by uptake of gas-phase species and heterogeneous reactions (Morales, 1986; Kim and Park, 2001; Park et al., 2004; Zhu et al., 2010).

The uptake of sulfate onto mineral dust is important both for dust properties and for the sulfur cycle. Freshly-emitted Sahara dust is very hydrophobic (Kaaden et al., 2009), whereas sulfate-coated mineral dust has increased CCN activity and may even act as “giant CCN” (Levin et al., 1996), while sulfate coatings reduce the ice nuclei activity of mineral dust (Cziczo et al., 2009; Pruppacher and Klett, 1997). Mineral dust is a particularly important source of iron in nutrient-limited open ocean waters, and chemical aging can reduce the pH of dust, increasing the solubility and bioavailability of iron (Jickells et al., 2005; Gasso et al., 2010; Rubasinghege et al., 2010; Kumar et al., 2010). Heterogeneous oxidation of SO₂ on dust can lead to reductions of >50 % in SO₂ concentration, and may account for 50–70 % of sulfate production in dust source regions (Dentener et al., 1996; Xiao et al., 1997; Zhu et al., 2010). Coagulation on to dust can also remove sulfuric acid aerosol and gas from the atmosphere. This means that dust reduces homogeneous nucleation of H₂SO₄ and changes the size distribution of sulfur towards coarse particles, reducing its lifetime compared to sulfate in finer particulate. It is estimated that heterogeneous reactions on mineral dust reduce sulfate and nitrate aerosol cooling near dust source regions by 0.5–1 W m⁻² (Dentener et al., 1996; Liao and Seinfeld, 2005). Understanding the uptake and oxidation of SO₂ on mineral dust is a key part of investigating the interactions and feedbacks between dust, sulfur, climate and clouds.

Sulfur isotopes have been used to investigate homogeneous and aqueous oxidation of SO₂ by OH, H₂O₂ and O₃ (Harris et al., 2012). Sulfur isotope abundances are described by the delta notation, which is the permil deviation of the ratio of a heavy isotope to the most abundant isotope (³²S) in the sample compared to a standard ratio:

$$\delta^x\text{S} (\text{‰}) = \left[\frac{\left(\frac{n(^x\text{S})}{n(^{32}\text{S})} \right)_{\text{sample}}}{\left(\frac{n(^x\text{S})}{n(^{32}\text{S})} \right)_{\text{V-CDT}}} - 1 \right] \times 1000 \quad (1)$$

where n is the number of atoms, ^xS is one of the heavy isotopes, ³³S, ³⁴S or ³⁶S, and V-CDT is the international sulfur isotope standard, Vienna Canyon Diablo Troilite, which has isotopic ratios of ³⁴S/³²S = 0.044163 and ³³S/³²S = 0.007877 (Ding et al., 2001). Isotopic fractionation is represented by the α value, which is the ratio of the heavy to the light isotope in the products divided by the ratio in the reactants:

$$\alpha_{34} = \frac{\left(\frac{n(^{34}\text{S})}{n(^{32}\text{S})} \right)_{\text{products}}}{\left(\frac{n(^{34}\text{S})}{n(^{32}\text{S})} \right)_{\text{reactants}}} \quad (2)$$

Values of α_{34} are characteristic for different reaction pathways and are therefore useful to investigate the different ox-

idation pathways for SO₂ on mineral dust in the laboratory and in the atmosphere.

This study presents measurements of the stable isotope fractionation of ³⁴S/³²S at room temperature (19 °C) during heterogeneous oxidation on dust surfaces and aqueous oxidation in dust leachate. The dust used is from the Sahara desert, which accounts for ~60 % of global dust emissions and loading (Tanaka and Chiba, 2006). The dust was collected on the Cape Verde islands (SDCV), and its mineralogy, composition and properties, as well as details on collection, are described in Coude-Gaussen et al. (1994) and Hanisch and Crowley (2001, 2003). We demonstrate that stable sulfur isotopes can be used to understand SO₂ oxidation on mineral dust both in the laboratory and in the field, and are particularly useful to investigate the roles of different minerals in surface oxidation and to quantify the importance of aqueous oxidation by transition metal ions in the atmosphere.

2 Background: uptake and oxidation of SO₂ by mineral dust

Uptake of SO₂ to mineral dust can occur via the reversible, physisorption pathway, or the irreversible, chemisorption pathway, which can be followed by oxidation of the sorbed sulfite. This study will only consider irreversible uptake, which can account for >98 % of uptake at low SO₂ concentrations (Adams et al., 2005; Goodman et al., 2001). The initial uptake coefficient on Sahara dust, $\gamma = 4 \times 10^{-5}$, is not dependent on RH, [SO₂] or O₃ (Crowley et al., 2010) which suggests SO₂ adsorption is the rate-limiting step, rather than subsequent reactions and oxidation (Ullerstam et al., 2002).

Oxidation of adsorbed S(IV) can follow a number of pathways: O₃ is a very efficient oxidant, and oxidation can also be catalysed by iron and manganese in dust (Usher et al., 2002; Ullerstam et al., 2002). NO₂(g) and surface nitrate have been observed to oxidise surface sulfite (Ullerstam et al., 2003), and oxidation to CaSO₄ occurs when calcite is exposed to SO₂ and O₂ (Al-Hosney and Grassian, 2005). Sulfate production has even been observed on MgO in the absence of O₂ and O₃, and was attributed to the highly basic character of four-coordinated O anions on steps and corners (Pacchioni et al., 1994; Goodman et al., 2001). In this study, SO₂ will always be exposed to dust in synthetic air, and the reaction time will be very long, so the oxidation of adsorbed sulfite to sulfate should be close to completion (Ullerstam et al., 2002).

The SO₂ removal rate on dry dust decreases significantly with exposure to SO₂ as saturation is approached, suggesting uptake will only be important for ~10 h after dust emission (Judeikis et al., 1978). However, active sites can be regenerated by exposure to high humidity for a number of reasons, for example carbonic acid dissociation and release as CO₂(g), increased mobility of surface ions leading to microcrystallite formation, and direct generation of new active sites (Ullerstam et al., 2002, 2003; Al-Hosney and Grassian,

Table 1. Composition and mineralogy of SDCV adapted from Hanisch and Crowley (2003) and Coude-Gaussen et al. (1994), respectively.

Elemental composition	O	Si	Al	Mg	Ca	Fe	Ti	K	Na	Mn	P	S
Concentration (mg g ⁻¹ dust)	556.9	172.4	72.9	24.1	28.0	89.4	21.1	16.2	12.2	1.8	2.0	0.9
Mineralogy of clay fraction	Kaolinite		Smectite		Swelling chlorite		Chlorite		Illite			
Abundance (%)	34.3		10.5		14.2		7.9		30.3			

2005; Li et al., 2006). IR absorption bands for adsorbed sulfate do not change upon exposure to humidity (Ullerstam et al., 2002, 2003). Saturation behaviour of SO₂ under exposure to UV light has not been measured, however irradiation prevents surface saturation for ozone uptake on TiO₂ (Nicolas et al., 2009). These results suggest that experimental conditions such as humidity, ozone and irradiation will change the quantity of SO₂ taken up and oxidised, while the initial uptake to form sorbed S(IV) is the rate-limiting step and is therefore expected to be the major factor controlling isotopic fractionation.

Aqueous oxidation by ions leached from dust may be a particularly important contributor to oxidation of SO₂ in the atmosphere, especially as sulfate production increases aerosol hygroscopicity and CCN activity, facilitating further aqueous SO₂ oxidation (Usher et al., 2002; Ullerstam et al., 2002, 2003; Li et al., 2006). The oxidative activity of leachates is due to catalysis by metal ions: Fe(III) is the most important of these ions, however comparison to experiments with pure Fe salts show trace ions such as Mn and Cr also make a significant contribution to catalytic activity (Tilly et al., 1991; Rani et al., 1992). Catalytic activity does not significantly change when the solid phase is filtered out of the leachate. This shows aqueous oxidation dominates over any surface effects of particles in the solution (Cohen et al., 1981; Rani et al., 1992), although, when aqueous iron and titanium oxide suspensions are irradiated, sulfate quantum yields $\gg 1$ have been observed due to desorption of $\cdot\text{SO}_3^-$ and initiation of a radical chain reaction (Hong et al., 1987; Faust et al., 1989).

Aqueous oxidation shows complex pH-dependence, as metal ions are more soluble but the more reactive SO₃²⁻ is less abundant at lower pH (Cohen et al., 1981; Rani et al., 1992). Dust is not the only contributor of transition metal ions for SO₂ oxidation: transition metals ions from anthropogenic sources are generally more soluble than ions in dust, and thus more available for reaction with S(IV) in solution (Kumar et al., 2010). The reaction pathways catalysed by anthropogenic and natural transition metal ions are the same once the ions are leached into solution, thus the fractionation factor measured for dust leachate in this paper will also be applicable to leachate from combustion products such as fly ash (Cohen et al., 1981).

3 Methods

3.1 Apparatus and experiments

3.1.1 Mineral dust used in experiments

The dust used in this study was Sahara dust collected from the Cape Verde islands (SDVC). Its mineralogy, composition and properties are described in Coude-Gaussen et al. (1994) and Hanisch and Crowley (2001, 2003) and summarised in Table 1. The non-clay fraction of the dust contains primarily quartz, feldspars and calcite. Sahara sand obtained directly from the Sahara desert has a mean diameter of $>150\ \mu\text{m}$ (Morales, 1986), whereas transported dust contains dust particles as small as 200 nm and has a mean diameter of $<10\ \mu\text{m}$ that decreases with distance transported (Heinold et al., 2009; Kaaden et al., 2009; Wagner et al., 2009; Morales, 1986). Thus, Sahara dust from the Cape Verde Islands is much more relevant to atmospheric chemistry than a local sand sample which would include very coarse grain sizes.

3.1.2 Aqueous oxidation in mineral dust leachate

Leachate representing 0.5 g of dust per 100 ml was prepared by soaking the dust for two days in MilliQ water. The solution was not open to the atmosphere during leaching, thus the pH of the leaching solution was 7. The liquid phase was then poured off the solid dust as aqueous oxidation has been shown not to be affected when the solid phase is removed (Cohen et al., 1981; Rani et al., 1992). The leachate was then stored in an air-tight jar in the dark at room temperature and used within two weeks. The leaching protocol was chosen to mimic ambient leaching, without sonication or heating, and provide a first estimate of sulfur isotope fractionation during aqueous oxidation in mineral dust leachate. No chemicals or buffers were added to the solution, in order to minimise interferences such as unwanted aqueous oxidants, although in the ambient environment it is likely that the cloud water in which leaching occurs will contain a number of other species. The concentrations of Al, Ca, Fe, Mg, Ba, Mn, Ti, Cr and Sr in the leachate were measured by inductively-coupled plasma optical emission spectrometry with a Perkin-Elmer Optima 3300 XL.

SO₂ gas (Linde AG, 102 ppm \pm 2 % in synthetic air) was diluted with synthetic air (Westfalen AG, 20.5 % O₂ in N₂) to 6.7 ppm and 13.3 ppm in a total flow of 600 sccm for experimental runs #1 and #2, respectively. This flow was

passed through 300 ml of leachate in a bubbler, followed by a bubbler containing 6 % H₂O₂ to collect residual SO₂ as described in Harris et al. (2012). PFA fittings and tubings were used for all gas flows. The experiments were run for ~8 h. Following each experiment, both bubblers were rinsed and BaCl₂ was added to precipitate sulfate as BaSO₄. The BaSO₄ was collected by filtration through Nuclepore track-etch polycarbonate membrane filters (Whatman Ltd.) with 0.2 μm pores, which had been coated with a 10 nm-thick gold layer using a sputter coater (Bal-tec GmbH, Model SCD-050) prior to sample collection. The experimental system and potential interferences were examined in detail by Harris et al. (2012) and will therefore not be discussed in this paper. Background sulfate sources considered in Harris et al. (2012), such as impurities in the water, have a negligible effect on the results as oxidation in the leachate is very efficient and a large amount of sulfate product is produced.

3.1.3 Heterogeneous oxidation on the Sahara dust surface at subsaturated humidity

Heterogeneous oxidation on mineral dust was investigated by passing 250 sccm of 4.2 ppm SO₂ gas in synthetic air through a dust-coated filter, as shown in Fig. 1. Dust was pipetted on to gold-coated Nuclepore filters (0.2 μm pore) in a 1:2 ethanol:water mixture, which helped the dust to adhere to the filter better than mounting in pure water. A mixed cellulose ester filter (Whatman GmbH) was placed under the Nuclepore filter to prevent tearing when gas flows were switched on and off. The mounted dust had a modal diameter of 2 μm with maximum grain diameters of ~8 μm, showing the dust was not significantly size-fractionated during mounting compared to the results of Coude-Gaussen et al. (1994). The reactor was made of glass with an FEP O-ring (Ralicks Industrie- und Umwelttechnik) connecting the two parts. PFA fittings and tubings were used for gas flows. SO₂ gas (Linde AG, 102 ppm ± 2 % in synthetic air) was diluted with synthetic air (Westfalen AG, 20.5 % O₂ in N₂) to the desired concentration before entering the reactor. A high concentration of SO₂ (4.2 ppm) was used to prevent significant isotopic changes to the residual SO₂. Less than 1 % of the SO₂ gas reacted to form sulfate in all experiments. The residual SO₂ gas was collected in some experimental runs as described in Harris et al. (2012) and the isotopic composition confirmed the SO₂ was not significantly altered during the experiments.

The reaction system was run under a variety of different experimental conditions, which are summarised in Table 2 along with abbreviations that will be used throughout this paper. Untreated dust was also examined as an experimental control to monitor background sulfate. A high power LED ($\lambda_{\text{max}} = 365$ nm, 50 mW at 350 mA, Roithner Lasertechnik GmbH) was used to irradiate the dust in four experiments through a Suprasil quartz window (Heraeus Quarzglas GmbH), which has a transmittance of >90 % between 200 and 1000 nm. The emission spectrum of the LED

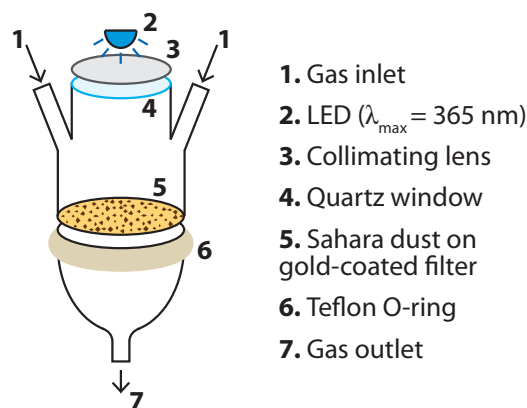


Fig. 1. Reactor used to investigate fractionation during oxidation of SO₂ on mineral dust.

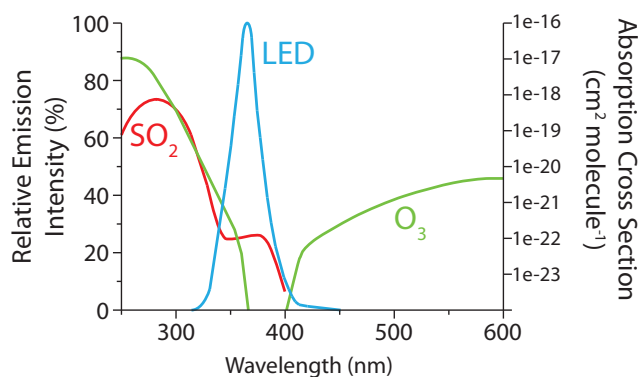


Fig. 2. Emission spectrum of LED used to irradiate mineral dust samples (blue line, left axis, Roithner (2011)) and absorption spectra of SO₂ (red line, right axis, Rufus et al., 2003) and O₃ (green line, right axis, Bogumil et al., 2003).

is shown in Fig. 2, along with the absorption spectra of O₃ and SO₂. Neither O₃ or SO₂ absorb significantly in the wavelength range of the LED, so no gas-phase photolytic reactions will occur. Humidity was added to the reaction chamber in four experiments by passing the synthetic air flow through MilliQ water to achieve a relative humidity of around 40 %, which would correspond to 2 monolayers of water on the dust (Gustafsson et al., 2005). The dust was not heated before use, so even samples with no added humidity will have surface-sorbed water molecules and inter-lamella water in the clay fraction. 20 ppm ozone was added to the gas mixture in four experiments by passing 100 sccm of the synthetic air flow over a low-pressure mercury vapour lamp (Jelight Company Inc., USA). The ozone concentration was measured with a Thermo Electron Corporation UV Photometric O₃ Analyzer (Model 49C). The rate of gas-phase SO₂ oxidation by O₃ is negligible (Li et al., 2006), no aqueous phase is present, and photolysis of SO₂ and O₃ is negligible, thus surface reactions will be solely responsible for sulfate production. Each experiment was done in duplicate with and without the addition

Table 2. Experiments to investigate isotopic fractionation during oxidation of SO₂ on the surface of mineral dust.

Abbreviation	O ₃	Light	Humidity	Run	Length (h)
MDdark	no	no	no	1	7.9
				2	7.2
MDO3	yes	no	no	1	7.9
				2	9.2
MDhv	no	yes	no	1	8.2
				2	8.2
MDO3hv	yes	yes	no	1	7.8
				2	7.7
MDRHdark	no	no	yes	1	7.8
				2	8.3
MDRHO3	yes	no	yes	1	7.5
				2	7.9
MDRHhv	no	yes	yes	1	6.7
				2	7.3
MDRHO3hv	yes	yes	yes	1	6.3
				2	7.5

of humidity, for a total of 16 experimental runs. The experiments were run for 6–9 h to generate sufficient sulfate for NanoSIMS isotopic analysis. Following each experiment, filters were stored in airtight boxes before being mounted for NanoSIMS and SEM analysis.

3.2 SEM analysis

A scanning electron microscope (SEM) was used to investigate the quantity of sulfate produced during the leachate experiments and the composition of individual dust grains in the different samples for the surface reaction experiments. The BaSO₄ and dust samples on gold-coated filters were directly analysed in the SEM without any further treatment. A LEO 1530 field emission SEM with an Oxford Instruments ultra-thin-window energy-dispersive X-ray detector (EDX) was used for the analyses. The SEM was operated with an accelerating voltage of 10 keV, a 60 μm aperture and a working distance of 9.6 mm. “High current mode” was used to increase the EDX signal and improve elemental sensitivity.

Before NanoSIMS analysis of the samples, the SEM was run in automatic mode and took 400 evenly-spaced images of each filter at 19 500× magnification. The EDX spectrum was measured with a 1 s integration time at 25 points on a 5×5 grid for each image, leading to 10 000 EDX measurements across each filter. For the leachate oxidation BaSO₄ samples, EDX signals were measured for O(K_α), Au(L_α), S(K_α) and Ba(L_α). The quantity of sulfate on each filter was then determined by estimating the background from both the Gaussian distribution of the gold signal and the quartile method, as described in Harris et al. (2012) and Winterholler (2007). This quantification method is ideal for NanoSIMS studies, as quantification is achieved without extra sample treatment and the limit of detection is very low. The precision is fairly

low (~40 %, decreasing with increasing BaSO₄ quantity due to Poisson statistics) and the method is not ideal for samples with a large amount of BaSO₄ due to the possibility of the sample flaking off the filter during mounting, thus isotope mass balance was also used to find the extent of reaction (see Sect. 4.1), as was used in Lin et al. (2011), Harris et al. (2012) and Derda et al. (2007).

During the analyses of the dust grains from the surface oxidation experiments, seven EDX channels were measured in automatic mode: Fe(L_α), Mg(K_α), Al(K_α), Si(K_α), S(K_α), Ca(K_α) and Ti(K_α). The background was subtracted from the signals using the quartile method (Harris et al., 2012; Winterholler, 2007). The signals were used to investigate the composition of the mineral dust and association of sulfate with the different elements in the dust. The SEM images were also used to measure the size distribution of the dust, as described in Winterholler (2007). The density of the dust was estimated to be 3.1 g cm⁻³ from the densities of the three main components, SiO₂, Al₂O₃ and FeO, and this was used to calculate the mass of dust on each filter. The BET surface area of the dust was measured by Hanisch and Crowley (2001) to be 1.5 m² g⁻¹ for grains with *d* < 10 μm.

Following NanoSIMS analysis, the dust grains from the surface oxidation experiments were again examined in the SEM, to determine the chemical composition of the dust grain for each NanoSIMS analysis point. Coordinate transfer was used to locate the grains in the SEM and an image and an EDX spectrum were then taken at each point. An example is shown in Fig. 3. Peaks were counted if they were more than three times the noise at the peak position (Goldstein et al., 1981), and an approximate height was measured by overlaying a grid as shown in the figure. The known composition of the dust (Hanisch and Crowley, 2003) was used to determine relative sensitivity factors (RSF) for the different elements based on the EDX measurements on unreacted dust grains. RSF values were in the expected range of 0.1 to 2 (Goldstein et al., 1981). An approximate atomic percentage for all detectable elements could then be estimated for each experimental grain. The error in atomic percentage was defined as ±1 unit on the overlaid scale, multiplied by the RSF for the element. The resulting composition obtained for each dust grain is not surface-sensitive as the X-rays are released from a depth of < 1 μm (Goldstein et al., 1981), so the results will show the elements present at the analysis point but will not be especially sensitive to the newly-produced sulfate from the experimental treatment.

3.3 NanoSIMS analysis

The sulfur isotopic composition was determined with the Cameca NanoSIMS 50 ion probe at the Max Planck Institute for Chemistry in Mainz (Hoppe, 2006; Groener and Hoppe, 2006). The NanoSIMS 50 has high lateral resolution (< 100 nm) and high sensitivity and can simultaneously measure up to five different masses through a multicollection

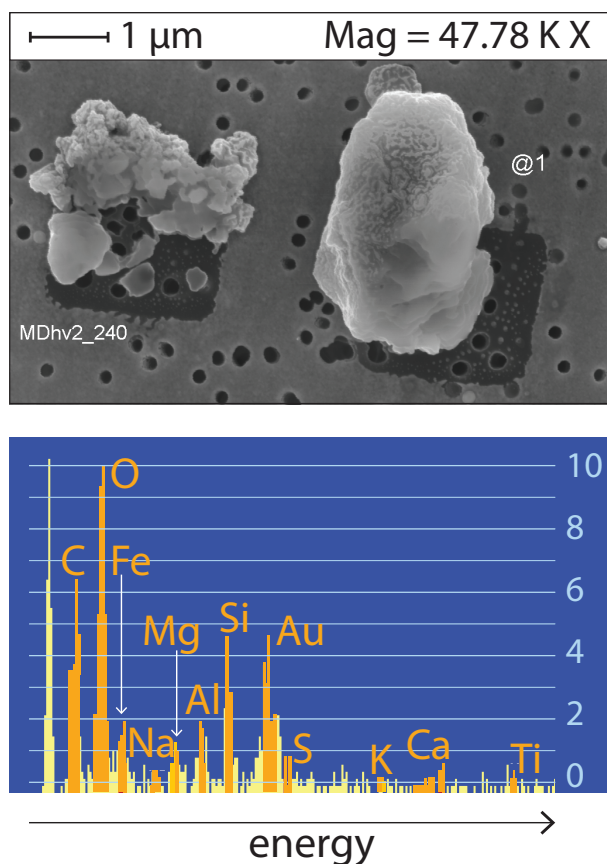


Fig. 3. SEM and EDX analysis of a mineral dust grain (right-hand grain) following a NanoSIMS measurement. The dark squares on the filter in the SEM image show where the NanoSIMS analysis has sputtered away the gold-coating. In the SEM EDX spectrum, element windows are highlighted in orange while the background is shown in yellow.

system, allowing high precision analysis of the small sample quantities required for this study. The use of this instrument to analyse sulfur isotope ratios is described in detail elsewhere (Winterholler et al., 2006, 2008) and the analysis conditions are described in Harris et al. (2012), so only a brief description will be given here.

The samples are analysed directly on the gold-coated Nuclepore filters without further processing. Samples with a particularly high BaSO₄ loading and all dust samples are gold-coated on top of the sample before NanoSIMS analysis to prevent excessive charging. A ~ 1 pA Cs⁺ beam is focussed onto a ~ 100 nm sized spot and rastered in a $2 \mu\text{m} \times 2 \mu\text{m}$ grid over the grain of interest. The ejected secondary ions are carried into the mass spectrometer and multicollection system. For the BaSO₄ from leachate oxidation experiments, each measurement consists of 200–400 cycles of 4.096 s duration preceded by varying lengths of presputtering until the gold coating (if present) is removed and the count rate is stable. For the surface oxidation samples, the

sulfate produced in the experiments will be on the surface of the particles, so analyses were fairly short and presputtering was kept to a minimum: each measurement consisted of 120 cycles of 4.096 s duration, and presputtering and beam centering were carried out on an area of at least $10 \mu\text{m} \times 10 \mu\text{m}$ so that the surface was conserved for analysis.

The session instrumental mass fractionation (IMF) was determined with IAEA BaSO₄ standards SO5 and SO6, however the IMF for sulfate on mineral dust grains will also be dependent on the matrix. The major cation was determined from SEM-EDX analysis taken on individual grains after the NanoSIMS analysis, as described in the previous section, and the IMF correction relative to BaSO₄ was then applied according to Winterholler et al. (2008). The untreated Sahara dust (i.e. the Sahara dust as collected on the Cape Verde Islands and not subject to experimental exposure to SO₂) contained a measureable quantity of sulfate, so a background correction of the isotope ratio was needed for the surface oxidation samples. The effect of this was minimised by keeping analyses short so that primarily surface sulfate was analysed, however the background was still significant. 28 untreated grains were analysed to quantify the background sulfur isotope signal. The untreated grains had an average ³²S signal of 447 ± 385 counts per second and a $\delta^{34}\text{S}$ of 18.6 ± 5.9 ‰. This falls within the range of values previously reported for sediments in the Sahara desert (Drake et al., 2004) and Sahara dust collected in the North Atlantic (Winterholler et al., 2006). Thus, experimentally-treated grains were only considered in the data analysis if their ³²S signal was >900 counts s⁻¹, and values of $\delta^{34}\text{S}$ for these grains were corrected for the isotopic composition of the background. 102 experimental grains had high enough ³²S counts for useful isotopic information, and these were distributed fairly evenly across the different experiments, so that at least eight grains per sample gave useful information for each set of experimental conditions.

For each sample of the leachate experiments, at least five spots were measured and the weighted average and error was calculated, as described in Harris et al. (2012). The counting statistical error was typically 1–2 ‰ for each analysis spot and the overall error for each sample 2–5 ‰. For the surface oxidation experiments, the spot-to-spot error was added to the counting statistical error so that the measurements on each grain could be treated individually, rather than calculating an average for all grains on a particular sample filter. The spot-to-spot error of the SO5 and SO6 standards was used as an estimate of the spot-to-spot error for the measurement session, and this was then combined with the counting statistical error to determine the measurement uncertainty for each individual grain. For each individual grain, the counting statistical error was typically 4–5 ‰ and the overall error 5–6 ‰.

3.4 Positive matrix factorization

The composition of each grain from post-NanoSIMS SEM analysis was used as input for a Positive Matrix Factorization (PMF) model which was run with the software EPA PMF v3.0.2.2. This is a multivariate analysis tool which identifies “factor profiles” and “factor contributions” for data sets which have a large number of variables measured across many samples (Norris et al., 2008). Although the model is designed to identify source profiles and contributions to environmental data sets, it is ideal for this study as it allows data points to be individually weighted and it constrains results so that no “factor” can have a negative contribution to a sample.

Atomic percentages of O, Fe, Na, Mg, Al, Si, S, K, Ca and Ti were used as input for the model, as well as S isotope measurements from NanoSIMS analysis. When a peak was below the limit of detection, an atomic percentage of one third of the lowest measured concentration for the element was used, and the uncertainty was set to twice the normal uncertainty for the element to reduce the weighting of the point. All elements were classed as “strong” as the uncertainties did not need to be increased, however $\delta^{33}\text{S}$ was classified as a “weak” variable as its analysis in the NanoSIMS can be problematic due to counting statistics combined with topography and matrix effects. $\delta^{34}\text{S}$ was set as the “total variable”, leading to an automatic “weak” classification. The “Extra Modeling Uncertainty” was set to the recommended 5 % (Norris et al., 2008). No two elements showed any significant correlation.

A random seed was used to initiate the model and 20 base runs were performed. The model was run with three, four and five ‘factors’ and it was found that four ‘factors’ gave the most consistent results with the lowest Q (object function) value and the best resolution of elements and isotopic compositions. Only the four factor analysis will be discussed further. The model described the data adequately: the residuals were approximately normally distributed and only one scaled residual for one Al value was outside the $\pm 3\sigma$ limit. The overall profiles of the four identified factors varied only a small amount between the 20 model runs, and the dominant species in each factor remained the same in all 20 runs.

4 Aqueous oxidation in Sahara dust leachate

4.1 Catalytic activity of the solution and rate of reaction

The concentrations of various elements present in the leachate, measured with ICP-OES, are shown in Table 3. The leachate was extremely efficient at oxidising SO₂, thus the fractionation factor must be found by considering the Rayleigh equations, which describe the isotopic composition of products and residual reactants as a function of the fractionation factor and the fraction of reactant remaining unreacted (Mariotti et al., 1981; Krouse and Grinenko, 1991). The

Table 3. The concentrations of various elements present in Sahara dust leachate measured with ICP-OES. “Concentration” refers to the solution used to oxidise SO₂ in this study, which was made with 0.5 g of dust per 100 ml of water, while “ $\mu\text{g g}^{-1}$ dust” is the amount of the element that is soluble in 1 g of dust following 2 days in MilliQ water. “RSD” is the relative standard deviation of 3 measurements from the ICP-OES.

Element	Concentration (mol L ⁻¹)	$\mu\text{g g}^{-1}$ dust	RSD (%)
Al	3.19×10^{-5}	170	3.7
Mg	1.61×10^{-5}	77.1	3.1
Ca	1.53×10^{-5}	121	2.8
Fe	7.74×10^{-6}	85.2	8.4
Ba	2.64×10^{-6}	71.5	1.9
Ti	2.22×10^{-6}	20.9	1.3
Mn	7.48×10^{-7}	8.09	4.1
Sr	1.43×10^{-7}	2.47	0.95
Cr	6.2×10^{-8}	0.64	160
Ni	3.4×10^{-9}	0.04	840

fraction of SO₂ remaining was measured for each of the two experimental runs both with SEM quantification as described in Sect. 3.2 and by considering mass balance between the measured isotopic composition of the residual SO₂ and the product sulfate:

$$\delta^{34}\text{S}_i = f \cdot \delta^{34}\text{S}_{\text{SO}_2} + (1-f) \cdot \delta^{34}\text{S}_{\text{sulfate}} \quad (3)$$

where f is the fraction of reactant (SO₂) remaining and $\delta^{34}\text{S}_i$, $\delta^{34}\text{S}_{\text{SO}_2}$ and $\delta^{34}\text{S}_{\text{sulfate}}$ are the isotopic compositions of the initial SO₂ gas, residual SO₂ gas and product sulfate, respectively. For each experimental run both estimates differed by <1 %, and the two estimates were averaged to find the fraction remaining for each of the experimental runs.

The oxidation of SO₂ by mineral dust leachate was very efficient. >99 % of SO₂ was oxidised after passing through one bubbler, compared to the 39 % of SO₂ that is collected in one bubbler containing 6 % H₂O₂ and <1 % that is oxidised in a bubbler with 0.1 M Fe²⁺/Fe³⁺ (Harris et al., 2012). The fraction oxidised at [SO₂] = 6.7 ppm (99.8 %) was only slightly higher than the fraction oxidised at [SO₂] = 13.3 ppm (99 %), showing the leachate was not close to exhausting its oxidation capacity. Thus, it is clear iron is not the most important transition metal for the catalysis of SO₂ oxidation in mineral dust leachate solutions; other ions measured in the solution, such as manganese and chromium, are also highly active in oxidation. This is in agreement with the results of Tilly et al. (1991) and Rani et al. (1992), which showed that these ions do not just contribute independently to oxidation, but that mixtures of ions interact synergistically, resulting in greatly-enhanced oxidation rates. Thus, soluble iron alone is not a good indicator of SO₂ oxidising ability, which may explain why correlation between soluble Fe and

sulfate is often poor (Kumar and Sarin, 2010; Baker et al., 2006).

4.2 Fractionation of ³⁴S/³²S during aqueous oxidation in Sahara dust leachate

The fractionation factor can be found from the Rayleigh equation describing the δ³⁴S of the sulfate product with respect to the fraction of SO₂ oxidised (Mariotti et al., 1981; Krouse and Grinenko, 1991):

$$\alpha_{34} = \frac{\ln\left(1 - \left(\frac{R_p}{R_i}\right)(1 - f)\right)}{\ln f} \quad (4)$$

where R_p and R_i are the ratios of ³⁴S/³²S for the product sulfate and the initial SO₂ gas, respectively and f is the fraction of SO₂ remaining. The δ³⁴S of the sulfate formed in the leachate needs to be corrected for the contribution from sulfate that was leached from the dust itself. The effect of this correction on δ³⁴S_p was negligible as the leachate contained <1 μM of sulfate while the reaction added >200 μM of sulfate to the solution.

The fractionation factor can also be found from the Rayleigh equation describing the δ³⁴S of the residual SO₂ gas and the fraction of SO₂ oxidised (Mariotti et al., 1981; Krouse and Grinenko, 1991):

$$\alpha_{34} = \frac{\ln\left(\frac{R_r}{R_i}\right)}{\ln f} - 1 \quad (5)$$

where R_r and R_i are the ratios of ³⁴S/³²S for the residual SO₂ gas and the initial SO₂ gas, respectively and f is the fraction of SO₂ remaining. The measured δ³⁴S of the residual SO₂ was corrected for fractionation during collection in H₂O₂ as described in Harris et al. (2012).

Four estimates of α₃₄ were thus obtained: from the residual SO₂ and the product sulfate for each of the two experimental runs. The four measurements were averaged and the 1σ standard deviation taken as the error:

$$\alpha_{\text{leachate}} = 0.9917 \pm 0.0046 \quad (6)$$

at 19 °C. Fractionation was mass-dependent with regards to ³³S. The majority of the uncertainty in the fractionation factor is due to the uncertainty in the NanoSIMS measurements of the δ³⁴S values. The fractionation factor is not significantly different to the fractionation factor for the oxidation of SO₂ by a solution of Fe²⁺ and Fe³⁺ (α_{Fe} = 0.9894 ± 0.0043) measured by Harris et al. (2012). However, in agreement with previous studies (Cohen et al., 1981; Tilly et al., 1991; Rani et al., 1992), the quantity of sulfate produced (see Sect. 4.1) shows that iron is not the only transition metal present in leachate that is active in catalysing SO₂ oxidation. Concentrations of other transition metals in the leachate that are also available for reaction, such as Cr and Mn, are presented in

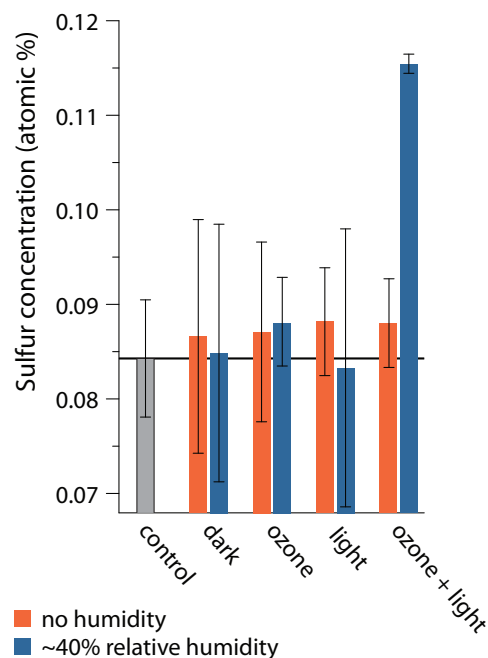


Fig. 4. Quantification of sulfate addition to mineral dust from surface SO₂ oxidation. “Control” shows the amount of sulfate present in untreated dust, and the labels on the x-axis refer to the different experimental conditions under which SO₂ was exposed to the dust. Error bars are the 1σ standard deviation from the Poisson distribution depending on the number of points with a significant signal.

Table 3. Thus, the identity of the metal catalysing SO₂ oxidation does not affect the sulfur isotope fractionation, which suggests fractionation is not due to the initiation reaction but the subsequent reactions in the chain (Herrmann et al., 2000). The average fractionation factor for transition metal-catalysed oxidation of SO₂ from the current and previous measurements is:

$$\alpha_{\text{TMI}} = 0.9905 \pm 0.0031 \quad (7)$$

5 Fractionation of ³⁴S/³²S during heterogeneous oxidation on Sahara dust surfaces

5.1 Quantification of sulfate production

Sulfate production on the dust surface at subsaturated humidity was quantified as described in Sect. 3.2, and the results are shown in Fig. 4 (abbreviations are defined in Table 2). Experiment lengths ranged from 6.3 to 9.2 h, so the results shown were corrected and represent the linearly-extrapolated concentration after exactly 8 h of experimental time, to facilitate comparison between experiments. The surface sulfate increase will be significantly more than the reported total atomic percentage increase, as EDX measurements are not surface-sensitive (Goldstein et al., 1981). As an estimate, for

a grain 2 μm in diameter with experimentally-produced sulfate added only to the top 20 nm of the grain surface, the sulfate concentration in the surface layer would increase by more than 1000 % for MDRHO3hv, rather than the 30 % increase when the whole grain volume is considered. The total amount of sulfate was seen to increase in all experiments except for MDRHhv, although all changes are within the statistical error of the SEM measurement except for MDRHO3hv. The count rates observed during NanoSIMS analysis show an increase for all treated samples compared to the control, and are also much higher for MDRHO3hv, in agreement with the SEM samples. Thus, sulfate production is significant, fairly slow and similar for all experiments except MDRHO3hv: this combination of conditions saw much more sulfate produced than the other experiments combined, showing ozone, light and water vapour interacted synergistically to oxidise SO₂ much more efficiently than any of these parameters alone.

5.2 Bulk elemental analysis of reactive particles

Correlations between the sulfur EDX signal and the EDX signal of other elements may provide information on which elements are most important for sulfate production. Automatic EDX points with sulfur and at least one other element above the background were therefore examined for correlations, in both the untreated and treated dust samples. Each sample had >100 EDX points with significant signals for sulfate and at least one other element, so correlations could be examined individually within each sample type. In untreated dust, correlations can indicate whether the sulfate present is primary and present in the Sahara source region, or whether it is secondary and results from uptake and reactions during transport to the Cape Verde Islands. S and Ti signals show a slight positive correlation ($R^2 = 0.35$) in the untreated samples, which suggests the sulfate is secondary: primary sulfate would be more likely to be associated with Ca and Mg due to clays and minerals such as gypsum (Caquineau et al., 2002).

Correlations on experimental samples were only seen for those runs with no ozone or irradiation: S on MDdark dust was weakly correlated with Ti and Fe ($R^2 = 0.19$ and 0.13 , respectively), while S on MDRHdark dust was strongly correlated with Ti and Ca ($R^2 = 0.66$ and 0.53 , respectively). No mineralogical information is provided in automatic EDX analysis, and it is likely that the lack of correlation in other samples is because element concentrations are a poor representation of element availability for reaction, rather than an indicator that sulfate is produced evenly across dust grains. The SEM-EDX analysis also has a resolution of only ~1 μm, and grain heterogeneity with regards to mineralogy on this scale (Falkovich et al., 2001) will obscure correlations in the SEM-EDX signal.

Elements which are associated with higher SO₂ oxidation rates can also be examined by looking at the elemental profile of dust grains (from post-NanoSIMS single-particle SEM-

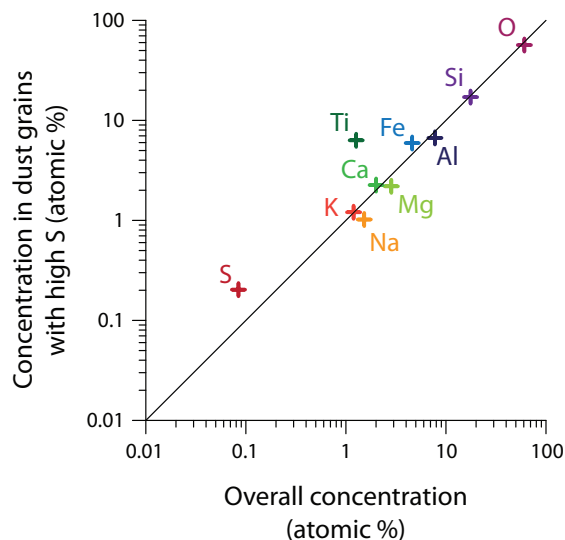


Fig. 5. Comparison of elemental composition of all dust and composition of dust with ³²S count rates high enough for reliable isotopic analysis.

EDX analysis) with high enough ³²S count rates for isotopic analysis, compared to the overall dust profile. This comparison is shown in Fig. 5. It can be seen that Ti is strongly enriched in oxidising dust, and K, Fe and Ca are slightly enriched, while Na, Mg, Al, Si and O show no relationship to oxidising ability of dust and only fall slightly below the 1 : 1 line because of mass balance. This is consistent with the correlations from automatic SEM analysis: Ti, Fe and Ca are the most important elements for oxidising ability, particularly in dark experiments where ozone and light are not available to facilitate further reaction pathways, while mineralogy is clearly the dominant factor controlling uptake.

5.3 ³⁴S/³²S fractionation on different dust components

The isotopic composition of sulfate on experimentally-treated samples was much more variable than on control grains, even within one set of experimental conditions. Variability within one set of experimental conditions was as large as overall variability of the data set. As atmospheric dust is strongly internally mixed with regards to mineralogy (Falkovich et al., 2001) most analysed grains will represent a mix of minerals, so a multivariate analysis model (described in Sect. 3.4) was used to examine the relationship between grain composition and isotopic fractionation. Four ‘factors’ were identified from the PMF analysis. Each ‘factor’ is not representative of a single mineral, but rather of a group of minerals that, acting together or separately, cause the same isotopic fractionation during sulfate formation; thus the ‘factors’ will hereafter be referred to as “mineral assemblages”. The elemental profiles of these factors are shown in Fig. 6. To determine the isotopic fractionation factor of the mineral assemblages, mineral assemblage contributions to sulfate for

Table 4. Fractionation of ³⁴S/³²S during heterogeneous oxidation of SO₂(g) on mineral dust surfaces. “Sulfate production” shows the percentage of the total sulfate production contributed by the mineral assemblage while “Reactivity” shows the amount of sulfate produced per gram of the minerals represented by the mineral assemblage per hour of reaction time at an SO₂ concentration of 4.2 ppm for MDRHO3hv experiments. γ is the reactive uptake coefficient considering the BET surface area of the dust for MDRHO3hv experiments.

Mineral Assemblage	Sulfate production (%)	Reactivity ($\mu\text{g sulfate/g minerals/h}$)	γ_{obs}	Mineralogy	α_{34}
1	85.0	12.6	3×10^{-5}	ilmenite + rutile	1.012 ± 0.010
2	3.2	0.40	9×10^{-7}	feldspar	0.948 ± 0.012
3	0.1	0.05	4×10^{-8}	silicates + basic components (e.g. MgO)	1.007 ± 0.011
4	11.7	2.91	9×10^{-6}	clay (chlorite, illite, smectite)	1.085 ± 0.013

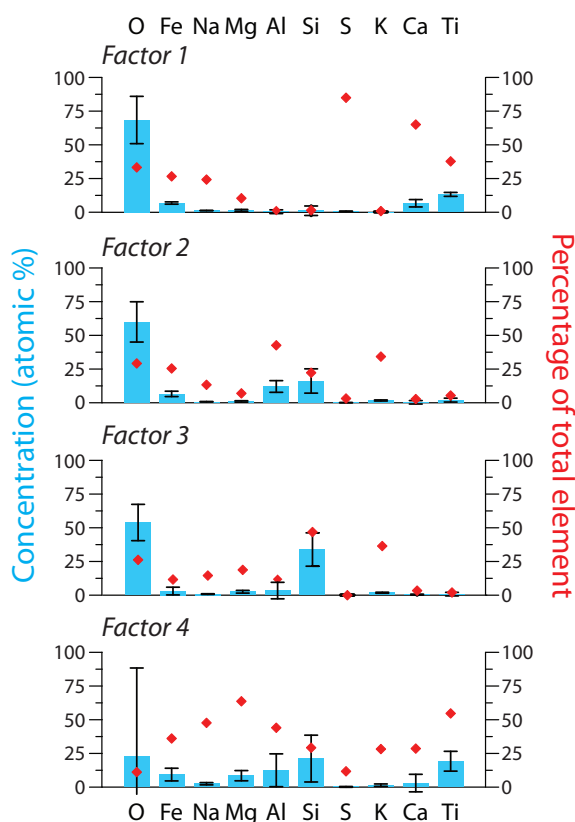


Fig. 6. Elemental profiles of the four “mineral assemblages” contributing to isotopic composition of sulfate produced from SO₂ oxidation, identified by PMF analysis. Columns with 1σ error bars (standard deviation of the results of 20 model runs) correspond to the left-hand axis and show the concentration of the element in atomic percent, while diamonds correspond to the right-hand axis and show the percentage of the element’s total concentration that is present in a particular mineral assemblage.

each grain were plotted against $\delta^{34}\text{S}$. The intercept where the mineral assemblage contribution was equal to one gave the fractionation factor α_{34} of the mineral assemblage. Fractionation was mass-dependent with regards to ³³S for all samples, thus fractionation of ³³S will not be discussed further.

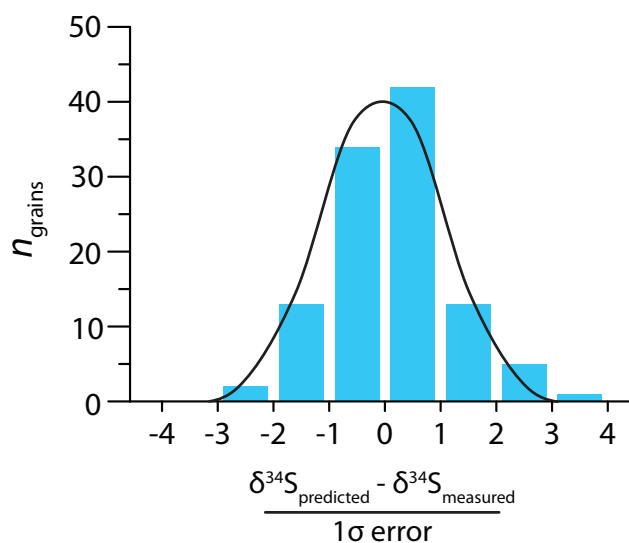


Fig. 7. Comparison of model accuracy (blue bars) with expected error from a normal distribution (black line).

The mineral assemblage α_{34} values were used to predict the $\delta^{34}\text{S}$ of the measured dust grains based on their composition, to test the fit between modelled and actual fractionation. The discrepancy between predicted and measured $\delta^{34}\text{S}$ was no greater than what would be expected from a normal distribution given the measurement error (Fig. 7), and the regression line weighted by the error in the measurements was ($R^2 = 0.62$):

$$\delta^{34}\text{S}_{\text{observed}} = (0.90 \pm 0.11)\delta^{34}\text{S}_{\text{predicted}} - (5.81 \pm 2.54) \quad (8)$$

which shows that the model fits the data well. However, this is not a rigorous test of the model as the same 102 measurements were used to generate the mineral assemblage α_{34} values and to test them, but it indicates the mineral assemblages are well-resolved with respect to isotopic fractionation.

Plots to determine fractionation factors were made for all samples together, as well as for sub-groups of samples to determine the role of experimental conditions in isotopic fractionation. The results are shown in Fig. 8. The error in the estimates of α_{34} for the sub-groups are much higher due to the

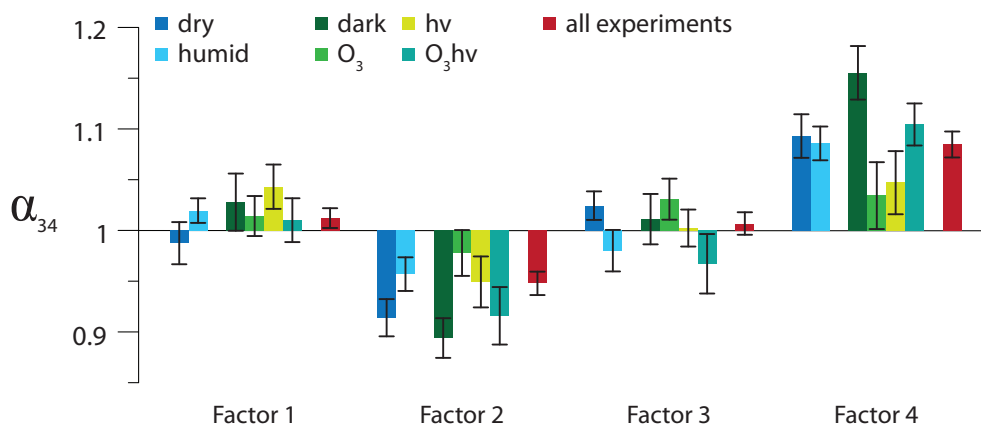


Fig. 8. Fractionation factors for $^{34}\text{S}/^{32}\text{S}$ for different mineral assemblages within Sahara dust: “dry” includes MDdark, MDO3, MDhv and MDO3hv, “humid” includes MDRHdark, MDRHO3, MDRHhv and MDRHO3hv; “dark” includes MDdark and MDRHdark, “hv” includes MDhv and MDRHhv, “O₃” includes MDO3 and MDRHO3, and “O₃hv” includes MDO3hv and MDRHO3hv. Error bars show the 1σ error.

much smaller number of measurements (47 and 55 grains for “all humid” and “all dry”, respectively; 20–31 grains for the effects of O₃ and light). The α_{34} could not be determined for individual experimental conditions (eg. MDO3 or MDRHhv) as the number of grains (8–14) was too small, thus the uncertainty in the result too large to be useful. It can be seen that presence or absence of humidity, light and ozone has much less effect on the isotopic fractionation than the dust composition: fractionation factors for different subsets generally agree with overall fractionation within the error for each mineral assemblage. This shows that isotopic fractionation is primarily due to uptake of SO₂(g) and not subsequent oxidation.

Based on the elemental profile of each mineral assemblage, its interaction with experimental conditions, and its reactivity, the mineralogical identity and reaction mechanism associated with each mineral assemblage was inferred. They are discussed in the following sections and summarised in Table 4. Several estimates of the oxidation rate for each mineral assemblage were obtained: the sulfate production percentage refers to the percentage of the total sulfate that was generated by that mineral assemblage during the experiment. The reactivity ($\mu\text{g sulfate g}^{-1} \text{ mineral h}^{-1}$) is the amount of sulfate produced per gram of the minerals represented by the mineral assemblage, divided by length of the experiment; the calculation does not consider decreases in rate due to saturation of the dust surface, and it is assumed that the surface fractions of the minerals are the same as the bulk fractions. This rate is relevant for the length of the experiments (6–9 h), but will eventually decrease as the dust is saturated. The reactivity could be used to estimate the rate of SO₂ oxidation and sulfate production on different dust types based on their mineral assemblages, however further investigation would be necessary given the strong role of mineral mixing in oxidation rate. The rate represented by the reactivity refers to the MDRHO3hv experiments, where the largest amount of sul-

fate was produced; oxidation under all other conditions is on average $16 \times$ slower and the uncertainty is much greater.

The reactivity and the BET surface area were used to estimate the reactive uptake coefficient γ for the dust according to Jayne et al. (1990):

$$\gamma_{\text{obs}} = \frac{4F_{\text{g}} \Delta n}{\bar{c}A n} \quad (9)$$

where F_{g} is the carrier gas flow rate ($\text{cm}^3 \text{ s}^{-1}$), \bar{c} is the mean thermal velocity (cm s^{-1} ; $\sqrt{\frac{3k_{\text{B}}T}{m}}$), A is the total droplet surface area (cm^2) and $\frac{\Delta n}{n}$ is the reduction in gas concentration. The γ_{obs} value found from this expression represents a combination of mass transfer, accommodation and reaction limitations, and provides only an estimate of the reactive uptake rate as it does not account for diffusion rate within the solid. The overall γ_{obs} for the dust, considering both reactive and non-reactive components, is 2.7×10^{-6} , which is ~ 1 order of magnitude lower than previously reported values (Crowley et al., 2010). This is well within the expected range considering the surface area of the dust is likely to be overestimated in this study as the dust is lying on a filter, rather than suspended in a flow reactor, and the previously reported values are for initial uptake coefficients before uptake slows due to aging and saturation. The dust in this study is a good representation of atmospheric dust that has already been aged, as it was transported from the Sahara desert to the Cape Verde Islands before being collected for use in experiments.

5.3.1 Mineral assemblage 1

Mineral assemblage 1 has a fractionation factor of $\alpha_{34} = 1.012 \pm 0.010$ which shows no significant variation depending on experimental conditions. It has high concentrations of Fe and Ti (6.8 and 13.2 at. %, respectively) and the highest reactivity of any mineral assemblage – contributing 85 % of sulfate production – which is in agreement with observations

of relatively high uptake coefficients for SO₂ on TiO₂ and on iron oxides and oxyhydroxides (Zhang et al., 2006; Crowley et al., 2010). The co-occurrence of Fe and Ti suggests that the mineral assemblage is representative of ilmenite, with some degree of weathering towards pseudorutile and rutile accounting for the excess Ti (Janssen et al., 2007; Putnis, 2002). Ilmenite is a chemically stable mineral that would be likely to have survived transport from the Sahara to the Cape Verde Islands and aging while on the Cape Verde Islands prior to collection (Janssen et al., 2007). The importance of Ti in the most reactive mineral assemblage agrees with the EDX sulfur correlation results from Sect. 5.2 which found Ti to be enriched in areas where sulfate production was highest.

As the uptake of SO₂, rather than the oxidation, controls isotopic fractionation, the coordination mechanism for SO₂ should relate to the isotopic fractionation. Given that the α is robust to experimental conditions and well-resolved for Mineral assemblage 1, the fractionation factor on the rutile (TiO₂) and on the parent ilmenite are the same. Hematite, goethite, magnetite and TiO₂ have all been shown to chemisorb SO₂ to a bidentate complex, with similar IR spectral bands observed for the adsorbed compounds where available. This suggests these three iron oxides will also have the same value for α as TiO₂ and by extension the same α as ilmenite (Fu et al., 2007; Zhang et al., 2006; Usher et al., 2002). Mineral assemblage 1 also has a significant amount of Ca. This may be due to formation of CaSO₄ from collocated Ca²⁺, possibly as the sample dries when it is put under vacuum for analysis. It is unlikely that CaO or CaCO₃ are directly taking up sulfate as the mechanisms of uptake (monodentate and direct reaction, respectively) are very different to iron and titanium oxides, and would not be expected to show the same fractionation factor (Usher et al., 2002).

In summary, ilmenite and its weathering product rutile are the most active components in SO₂ uptake in Sahara dust, and chemisorb SO₂ to a bidentate complex with a fractionation factor of $\alpha_{34} = 1.012 \pm 0.010$, which is expected to also represent fractionation on hematite, goethite and magnetite. Sulfate production was calculated to be 12.64 μg per mg of iron and titanium oxides and their weathering products per hour.

5.3.2 Mineral assemblage 2

Mineral assemblage 2 contributes 3.2 % of total sulfate production, and produces sulfate that is strongly depleted in ³⁴S. The elemental composition suggests the mineral assemblage represents feldspar and a component containing Fe such as mica or hematite, both of which are known to be common constituents of Sahara dust (Coude-Gaussen et al., 1994; Glaccum and Prospero, 1980). Al₂O₃ alone can have a relatively high uptake coefficient if it is basic in character (Judeikis et al., 1978; Crowley et al., 2010), while SiO₂ and acidic Al₂O₃ have very low uptake coefficients (Zhang et al., 2006). Uptake to this factor is relatively slow, and the

isotopic fractionation is opposite in direction the other factors, which have more basic character, thus uptake to Factor 2 appears to be dominated by less basic sites associated with Al. This is consistent with the expected effects of ageing during transport, which will remove alkali components, leaving aluminium oxides exposed. The Fe ions in the minerals associated with feldspar will increase the acidic character. Although Fe³⁺ can catalyse S(IV) oxidation (Herrmann et al., 2000), this reaction pathway will be insignificant without an aqueous phase. The adsorption of SO₂ to Al₂O₃ results in sulfite with significantly different IR absorption bands to, for example, MgO (Goodman et al., 2001), which explains the strongly negative isotope fractionation that is very distinct from the other factors.

In summary, aluminium oxide sites associated with feldspars, a common constituent of Sahara dust, take up SO₂ with a fractionation factor of $\alpha_{34} = 0.948 \pm 0.012$, which is also expected to be the fractionation factor for adsorption on to pure aluminium oxides. The sulfate production due to this factor is 0.40 μg of sulfate per mg of feldspar and aluminium oxide per hour.

5.3.3 Mineral assemblage 3

The isotope fractionation produced by Mineral assemblage 3 was slightly positive and very similar to Mineral assemblage 1. The contribution of Mineral assemblage 3 to total sulfate formation was minor (0.1 %). The elemental composition of Mineral assemblage 3 shows that it is primarily composed of quartz, as well as olivine and pyroxene, which are expected to be major components in Sahara dust (Coude-Gaussen et al., 1994; Glaccum and Prospero, 1980). However, pure SiO₂ has been measured to have very low or no reactivity with SO₂(g) in the laboratory (Zhang et al., 2006; Usher et al., 2002, respectively). Li et al. (2007) found that the addition of MgO to NaCl resulted in an increase in reactivity towards SO₂ larger than that expected from the individual uptake coefficients, and Zhang et al. (2006) also found excess reactivity in a mixture of continental crust components such as SiO₂ and MgO. Factor 3 contains a significant amount of Mg as well as other cations so it is likely mixing of SiO₂ and components with basic character, such as magnesium oxides or olivine, has increased the reactivity of the quartz fraction of the dust to a significant level. Spectra and adsorption mechanisms for SO₂ on silicates are not available, but the similarity of the fractionation factor for Mineral assemblage 3 to that of Mineral assemblage 1 suggests a similar, but much slower, adsorption mechanism.

In summary, adsorption of SO₂ to mixtures of quartz and components with basic character results in a fractionation factor of $\alpha_{34} = 1.007 \pm 0.011$. The total sulfate production is 0.05 μg of sulfate per mg of quartz per hour.

5.3.4 Mineral assemblage 4

Mineral assemblage 4 contributes 11.7% to the total sulfate production and produces sulfate strongly enriched in ³⁴S. The elemental profile shows that the mineral assemblage represents clays, particularly smectite, illite and chlorite, which have been shown to be major components of the clay fraction of Sahara dust from the Cape Verde Islands (Coude-Gaussen et al., 1994). Interlayer cations such as Mg²⁺, Ca²⁺ and Na⁺ are likely to be the components most available for reaction with SO₂, which is consistent with the correlation between Ca and sulfate presented in Sect. 5.2. Uptake of SO₂ by MgO and CaO has a relatively high rate (Crowley et al., 2010; Usher et al., 2002; Zhang et al., 2006), however DRIFTS IR absorption bands for sorbed S(IV) suggest sulfite is adsorbed quite differently on CaO and MgO (Low et al., 1971; Goodsell et al., 1972) so it is unlikely the adsorption to interlayer cations in clays can be represented by adsorption to oxides. SO₂ will react directly with CaCO₃ to produce CaSO₃ which is readily oxidised to CaSO₄ (Al-Hosney and Grassian, 2005; Li et al., 2006), and an analogous reaction with interlayer Ca and Mg is most likely the cause of SO₂ uptake in Mineral assemblage 4. Mineral assemblage 4 also has a large amount of Ti, however the fractionation factor is not in agreement with Ti uptake from Mineral assemblage 1. The calculated α_{34} for Mineral assemblage 4 is lower, i.e. closer to the α_{34} of Mineral assemblage 1, when the dust is exposed to O₃ or light, thus it appears that Ti associated with clay can only significantly contribute to SO₂ oxidation when the reaction is facilitated by light or O₃.

In summary, adsorption of SO₂ to interlayer cations, particularly Ca²⁺ and Mg²⁺, in clays such as smectite results in a strongly positive fractionation of $\alpha_{34} = 1.085 \pm 0.013$. Sulfate production is 2.91 μg per mg of clay minerals per hour of reaction time.

5.4 Overall ³⁴S/³²S fractionation on Sahara dust

The total average fractionation factor for heterogeneous SO₂ oxidation on the surface of Sahara dust can be estimated by two methods. The weighted average of all 102 individual NanoSIMS measurements results in a $\delta^{34}\text{S}$ of $9.5 \pm 3.9\%$. The average composition from the PMF, found by weighting the α_{34} values from the different mineral assemblages by their uptake efficiency and contribution to the total dust mass, is $\delta^{34}\text{S} = 10.1 \pm 9.9\%$. The two values agree very well and can be combined to estimate the average fractionation for the heterogeneous oxidation of SO₂ on the surface of Sahara dust:

$$\alpha_{\text{net}} = 1.0096 \pm 0.0036 \quad (10)$$

This average fractionation factor is only relevant for the particular dust sample measured in this study. The sulfur isotope fractionation factor for different dust sources should be calculated based on the mineral assemblage-specific fraction-

ation factors and the mineralogy and ageing of the dust of interest.

5.5 Sensitivity of sulfate production and isotopic fractionation to O₃, light and humidity

As discussed in the preceding sections, isotopic fractionation shows little sensitivity to the parameters that were varied between experiments. The relative contributions of the four mineral assemblages to sulfate production were also not significantly affected by the experimental conditions. This shows chemical composition and mineralogy of a dust grain are the most important parameters causing differences in isotopic fractionation, with the experimental conditions playing a secondary role. Isotopic fractionation will be controlled by the rate-limiting step, as the fraction reacted for other reaction steps will be ~ 1 , meaning that isotopic selectivity in these steps will not have an effect on the final product. The various experimental parameters would be likely to affect oxidation of adsorbed S(IV) but have less effect on initial uptake (Judeikis et al., 1978; Adams et al., 2005), thus the results of this study are consistent with previous laboratory studies, which have determined that SO₂ adsorption is the rate-limiting step for SO₂ uptake and oxidation on mineral dust (Ullerstam et al., 2002; Li et al., 2006).

The experimental parameters will affect the saturation behaviour of the dust, however in most experiments the oxidation rate was low and the dust was not exposed to SO₂ long enough to reach saturation (Mamane and Gottlieb, 1989). However, when the dust is exposed to humidity, light and ozone simultaneously (MDRHO3hv), the quantity of sulfate produced is >7 times higher than in any other experiment. Humidity regenerates the reactive capacity of dust for SO₂ uptake (Judeikis et al., 1978; Ullerstam et al., 2002), possibly due to the increased mobility of surface ions which leads to the re-exposure of active sites (Al-Hosney and Grassian, 2005). Uptake and decomposition of ozone, which increases the basicity and oxidising capacity of the surface, is highest when irradiated and at around $\sim 35\%$ RH (Hanisch and Crowley, 2003; Nicolas et al., 2009). Many components of dust, particularly iron and titanium oxides, are photosensitive and show increased uptake and oxidation due to the formation of electron-hole pairs (Nicolas et al., 2009; Ndour et al., 2009; Rubasinghe et al., 2010). The photoreactivity of Ti is supported by the lower fractionation factor for Mineral assemblage 4 when exposed to O₃ or light as discussed in Sect. 5.3.4. There is no significant change in isotopic fractionation within any mineral assemblage for the MDRHO3hv experiments, thus the increased sulfate production is not related to a change in mechanism. The combination of humidity, ozone and irradiation increases the rate of SO₂ oxidation, causing it to approach saturation. The experimental parameters can then have a significant impact on counteracting saturation of SO₂ uptake on dust, thus increasing the amount of SO₂ taken up and oxidised on the dust

during the experiments. The rate of uptake and oxidation is then approximately an order of magnitude higher than with any parameter alone.

6 Comparison to field studies

A number of studies have looked at isotopic ratios of sulfate in order to understand sulfur sources and oxidation pathways. As sulfur isotope fractionation factors have not been available for data interpretation, $\Delta^{17}\text{O}$ values are generally used to examine oxidation pathways. Oxidation by OH radicals and O₂ (which acts as the oxidant during transition metal catalysis) result in sulfate with $\Delta^{17}\text{O} = 0\%$, while oxidation by O₃ and H₂O₂ produces sulfate with $\Delta^{17}\text{O} = 8.8$ and 0.8% , respectively (Savarino et al., 2000; Lee and Thiemens, 2001). Alexander et al. (2003) used $\Delta^{17}\text{O}$ measurements of sulfate in East Antarctic ice cores to show that oxidation by O₃ and H₂O₂ was less important in glacial periods than in the surrounding interglacials. $\delta^{34}\text{S}$ of sulfate is also lower during glacial periods, thus Harris et al. (2012) proposed an increase in transition-metal catalysed SO₂ oxidation due to increased dust loads in glacial periods, based on laboratory measurements of oxidation of SO₂ by Fe²⁺/Fe³⁺ solutions. The results of this study show that sulfur isotope fractionation during oxidation by real mineral dust leachate is equal to fractionation during oxidation by iron catalysis, although oxidation is much faster, thus supporting the hypothesis that oxidation by transition metal catalysis is $\sim 27\%$ more important in glacial periods than in interglacial periods due to increased dust loads. Similarly, McCabe et al. (2006) measured $\Delta^{17}\text{O}$ of sulfate aerosol in Alert, Canada, and proposed that the importance of transition metal-catalysed oxidation was underestimated in winter, when concentrations of Fe and Mn are approximately doubled due to transport of polluted air masses. Norman et al. (1999) found that $\delta^{34}\text{S}$ of non-sea salt sulfate aerosol at Alert was lower in winter than in summer, which is consistent with the results of McCabe et al. (2006) when the fractionation factor for transition metal catalysis measured in this study is considered. Although the suite of transition metals from a polluted source will be different to those from a dust source, this study has shown that the identity of the transition metals involved in catalysis does not affect the isotopic fractionation.

In the majority of field studies, measured $\delta^{34}\text{S}$ of SO₂ is lower than $\delta^{34}\text{S}$ of sulfate (eg. Saltzman et al., 1983; Mukai et al., 2001; Novak et al., 2001). Thus, considering the fractionation factors from this study and from Harris et al. (2012), isotopic measurements are in agreement with modelling studies which show that transition metal catalysed oxidation of SO₂ contributes a minor part of global sulfate production. For example, Sofen et al. (2011) suggest the pathway contributes 18% of sulfate production globally. Using the present-day partitioning between oxidation pathways from Sofen et al. (2011) and the sulfur isotope fractiona-

tion factors from this study and from Harris et al. (2012), we would predict a global average difference of $+4.7\%$ between $\delta^{34}\text{S}$ of SO₂ and $\delta^{34}\text{S}$ of sulfate. Considering a number of studies that simultaneously measured $\delta^{34}\text{S}$ of SO₂ and sulfate (Saltzman et al., 1983; Mayer et al., 1995; Krouse et al., 1991; Tanaka et al., 1994; Torfs et al., 1997; Mukai et al., 2001; Novak et al., 2001), the best estimate of the globally-averaged difference between $\delta^{34}\text{S}$ of SO₂ and $\delta^{34}\text{S}$ of sulfate is $+2.8 \pm 3.1\%$; this would require 36% of oxidation to come from transition metal ion catalysis if the relative proportions of the other pathways remained the same. However, the area covered by these studies is mainly in Europe and North America, and there are no measurements from the polar regions and the Southern Hemisphere, so the result may not be representative of the true global picture. There are currently no regional studies focussing on the sulfur isotopic composition of sulfate formed on dust, although there are a number of field studies that have confirmed the important role dust can play in regional sulfur cycles (Falkovich et al., 2001; Umann et al., 2005; Sullivan et al., 2007). The importance of uptake at lower relative humidities is not well known, and although it is slow compared to aqueous oxidation, its climatic role may be underestimated as dust does not generally encounter high humidity until some days after emission (Dentener et al., 1996). A recent study by Alexander et al. (2012) considers the O-isotope composition of sulfate on one marine sample with an air mass of Saharan origin. The results show the importance of the O₃ oxidation pathway, while oxidation on the dust surface and in leachate in the aqueous phase in clouds contribute a small but significant amount of sulfate; the sulfur isotope fractionation factors presented in this study would be an ideal way to complement the $\Delta^{17}\text{O}$ analyses presented by Alexander et al. (2012). The fractionation factors presented in this study provide a new tool through which sulfur isotope measurements can be used to examine global and regional sulfur cycles, particularly the role of oxidation on clay minerals and in the aqueous phase.

7 Conclusions

The aim of this study was to measure fractionation of ³⁴S/³²S during oxidation of SO₂ by mineral dust leachate and on mineral dust surfaces, in order to better understand the role of SO₂ oxidation by mineral dust in the sulfur cycle. The fractionation factor α_{34} for oxidation in the leachate was $\alpha_{\text{leachate}} = 0.9917 \pm 0.0046$. Sulfate production was due to oxidation of SO₂ via the radical chain reaction pathway initiated by transition metal ions leached from the dust, and the oxidation rate was found to be more than 100× faster than oxidation by iron alone.

Heterogeneous oxidation on dry and humidified dust surfaces lead to isotopic fractionation that was controlled primarily by the dust composition and not by the reaction parameters: [O₃], irradiation, and humidity. However, almost

an order of magnitude more sulfate was produced when the dust was simultaneously exposed to SO₂, O₃, humidity and light. Fractionation from different reactions occurring within the same 2 μm² area was additive, thus a multivariate analysis model could predict δ³⁴S of the sulfate produced on the grains within expected experimental error. Not all particles reacted with SO₂, and the model identified the four major components of dust responsible for uptake and oxidation of SO₂. The most reactive components of dust were ilmenite, rutile and iron oxide, which produced sulfate with a fractionation factor of $\alpha_{34} = 1.012 \pm 0.010$. The overall fractionation factor on SDCV is $\alpha_{\text{het}} = 1.0096 \pm 0.0036$. Since the isotopic fractionation is controlled by the mineralogy of the dust, it will vary for dust from different dust source regions and between natural mineral dust and industrial dust sources.

The distinct fractionation factors for SO₂ oxidation by dust leachate – for example, in cloud droplets seeded on dust particles – and for uptake and oxidation on dust at subsaturated relative humidity will be particularly useful to investigate the relative importance of these two pathways as dust is transported. Although the aqueous reaction is much faster, the surface reaction may be fast enough to be important when the dust encounters O₃ and 30–40% relative humidity in the daytime, whereas high enough humidities for aqueous oxidation are unlikely to be reached for several days following emission (Dentener et al., 1996). However, the isotopic fractionation during uptake and oxidation on Sahara dust surface, in particular on Ti and Fe oxides and silicates, does not significantly differ from the isotopic fractionation during gas phase oxidation of SO₂ by OH and oxidation by O₃ and H₂O₂ in the aqueous phase ($\alpha_{\text{OH}} = 1.0087 \pm 0.0007$ and $\alpha_{\text{aq}} = 1.0167 \pm 0.0019$; Harris et al. (2012)). Therefore, further from dust sources when high enough humidity for all of the possible oxidation pathways has been encountered, ambient observations for Sahara dust may only be capable of quantifying the contribution of leached transition metal ions and surface reactions on clay minerals to sulfate formation. The fractionation factor for SO₂ oxidation by transition metal catalysis is distinct from oxidation on the dust surface, other than feldspar minerals, and by H₂O₂ and O₃ in the aqueous phase and OH in the gas phase, and will provide a means to assess the global and regional importance of transition metal-catalysed SO₂ oxidation, by both dust TMIs and anthropogenic TMIs, which cannot be easily predicted from measurable parameters such as soluble iron concentration. Oxidation on feldspar minerals was found to be slow and would only present a minor interference for these calculations.

Acknowledgements. We thank Elmar Gröner for his support with the NanoSIMS analyses, Joachim Huth for his help with the SEM/EDX analyses, Robert Oswald for assistance in measuring O₃ concentrations and Christa Sudek for help with the ICP-OES analysis. This research was funded by the Max Planck Society and the Max Planck Graduate Centre.

The service charges for this open access publication have been covered by the Max Planck Society.

Edited by: M. Ammann

References

- Adams, J. W., Rodriguez, D., and Cox, R. A.: The uptake of SO₂ on Saharan dust: a flow tube study, *Atmos. Chem. Phys.*, 5, 2679–2689, doi:10.5194/acp-5-2679-2005, 2005.
- Al-Hosney, H. A. and Grassian, V. H.: Water, sulfur dioxide and nitric acid adsorption on calcium carbonate: a transmission and ATR-FTIR study, *Phys. Chem. Chem. Phys.*, 7, 1266–1276, 2005.
- Alexander, B., Thiemens, M. H., Farquhar, J., Kaufman, A. J., Savarino, J., and Delmas, R. J.: East Antarctic ice core sulfur isotope measurements over a complete glacial-interglacial cycle, *J. Geophys. Res.-Atmos.*, 108, 4786, doi:10.1029/2003JD003513, 2003.
- Alexander, B., Allman, D. J., Amos, H. M., Fairlie, T. D., Dachs, J., Hegg, D. A. and Sletten, R. S.: Isotopic constraints on the formation pathways of sulfate aerosol in the marine boundary layer of the subtropical northeast Atlantic Ocean, *J. Geophys. Res.-Atmos.*, 117, D06304, doi:10.1029/2011JD016773, 2012.
- Baker, A. R., Jickells, T. D., Witt, M., and Linge, K. L.: Trends in the solubility of iron, aluminium, manganese and phosphorus in aerosol collected over the Atlantic Ocean RID D-1233-2011 RID B-2210-2010 RID B-8095-2008, *Mar. Chem.*, 98, 43–58, doi:10.1016/j.marchem.2005.06.004, 2006.
- Bogumil, K., Orphal, J., Homann, T., Voigt, S., Spietz, P., Fleischmann, O. C., Vogel, A., Hartmann, M., Kromminga, H., Bovensmann, H., Frerick, J., and Burrows, J. P.: Measurements of molecular absorption spectra with the SCIAMACHY pre-flight model: instrument characterization and reference data for atmospheric remote-sensing in the 230–2380 nm region, *J. Photochem. Photobiol. A*, 157, 167–184, 2003.
- Caquineau, S., Gaudichet, A., Gomes, L., and Legrand, M.: Mineralogy of Saharan dust transported over northwestern tropical Atlantic Ocean in relation to source regions, *J. Geophys. Res.-Atmos.*, 107, 4251, doi:10.1029/2000JD000247, 2002.
- Cohen, S., Chang, S. G., Markowitz, S. S., and Novakov, T.: Role of fly ash in catalytic oxidation of sulfur(IV) slurries, *Environ. Sci. Technol.*, 15, 1498–1502, doi:10.1021/es00094a013, 1981.
- Coude-Gaussens, G., Rognon, P., and Le Coustumer, M.: Incorporation progressive de poussières sahariennes aux limons des Iles orientales du Cap Vert, *C. R. Acad. Sci. II A*, 319, 1343–1349, 1994.
- Crowley, J. N., Ammann, M., Cox, R. A., Hynes, R. G., Jenkin, M. E., Mellouki, A., Rossi, M. J., Troe, J., and Wallington, T. J.: Evaluated kinetic and photochemical data for atmospheric chemistry: Volume V – heterogeneous reactions on solid substrates, *Atmos. Chem. Phys.*, 10, 9059–9223, doi:10.5194/acp-10-9059-2010, 2010.
- Cziczo, D. J., Froyd, K. D., Gallavardin, S. J., Moehler, O., Benz, S., Saathoff, H., and Murphy, D. M.: Deactivation of ice nuclei due to atmospherically relevant surface coatings, *Environ. Res. Lett.*, 4, 044013, doi:10.1088/1748-9326/4/4/044013, 2009.

- Dentener, F. J., Carmichael, G. R., Zhang, Y., Lelieveld, J., and Crutzen, P. J.: Role of mineral aerosol as a reactive surface in the global troposphere, *J. Geophys. Res.-Atmos.*, 101, 22869–22889, 1996.
- Derda, M., Chmielewski, A. G., and Licki, J.: Sulphur isotope compositions of components of coal and S-isotope fractionation during its combustion and flue gas desulphurization, *Isot. Environ. Health S.*, 43, 57–63, 2007.
- Ding, T., Valkiers, S., Kipphardt, H., De Bievre, P., Taylor, P. D. P., Gonfiantini, R., and Krouse, R.: Calibrated sulfur isotope abundance ratios of three IAEA sulfur isotope reference materials and V-CDT with a reassessment of the atomic weight of sulfur, *Geochim. Cosmochim. Ac.*, 65, 2433–2437, 2001.
- Drake, N. A., Eckardt, F. D., and White, K. H.: Sources of sulphur in gypsiferous sediments and crusts and pathways of gypsum redistribution in Southern Tunisia, *Earth Surf. Proc. Land.*, 29, 1459–1471, doi:10.1002/esp.1133, 2004.
- Falkovich, A. H., Ganor, E., Levin, Z., Formenti, P., and Rudich, Y.: Chemical and mineralogical analysis of individual mineral dust particles, *J. Geophys. Res.-Atmos.*, 106, 18029–18036, 2001.
- Faust, B. C., Hoffmann, M. R., and Bahnemann, D. W.: Photocatalytic oxidation of sulfur-dioxide in aqueous suspensions of alpha-Fe₂O₃, *J. Phys. Chem.*, 93, 6371–6381, 1989.
- Fu, H. B., Wang, X., Wu, H. B., Yin, Y., and Chen, J. M.: Heterogeneous uptake and oxidation of SO₂ on iron oxides, *J. Phys. Chem. C*, 111, 6077–6085, doi:10.1021/jp070087b, 2007.
- Gasso, S., Grassian, V. H., and Miller, R. L.: Interactions between mineral dust, climate, and ocean ecosystems, *Elements*, 6, 247–252, doi:10.2113/gselements.6.4.247, 2010.
- Glaccum, R. A. and Prospero, J. M.: Saharan aerosols over the tropical North Atlantic – mineralogy, *Mar. Geol.*, 37, 295–321, doi:10.1016/0025-3227(80)90107-3, 1980.
- Goldstein, J., Newbury, D. E., Echlin, P., Joy, D., Fiori, C., and Lifshin, E.: Scanning Electron Microscopy and X-ray Microanalysis, Plenum Press, New York, USA, 1–820, 1981.
- Goodman, A. L., Li, P., Usher, C. R., and Grassian, V. H.: Heterogeneous uptake of sulfur dioxide on aluminum and magnesium oxide particles, *J. Phys. Chem. A*, 105, 6109–6120, 2001.
- Goodsel, A. J., Low, M. J. D., and Takezawa, N.: Reactions of gaseous pollutants with solids. II. Infrared study of sorption of sulfur dioxide on magnesium oxide, *Environ. Sci. Technol.*, 6, 268–273, doi:10.1021/es60062a001, 1972.
- Groener, E. and Hoppe, P.: Automated ion imaging with the NanoSIMS ion microprobe, *Appl. Surf. Sci.*, 252, 7148–7151, doi:10.1016/j.apsusc.2006.02.280, 2006.
- Gustafsson, R. J., Orlov, A., Badger, C. L., Griffiths, P. T., Cox, R. A., and Lambert, R. M.: A comprehensive evaluation of water uptake on atmospherically relevant mineral surfaces: DRIFT spectroscopy, thermogravimetric analysis and aerosol growth measurements, *Atmos. Chem. Phys.*, 5, 3415–3421, doi:10.5194/acp-5-3415-2005, 2005.
- Hanisch, F. and Crowley, J. N.: Heterogeneous reactivity of gaseous nitric acid on Al₂O₃, CaCO₃, and atmospheric dust samples: a Knudsen cell study, *J. Phys. Chem. A*, 105, 3096–3106, 2001.
- Hanisch, F. and Crowley, J. N.: Ozone decomposition on Saharan dust: an experimental investigation, *Atmos. Chem. Phys.*, 3, 119–130, doi:10.5194/acp-3-119-2003, 2003.
- Harris, E., Sinha, B., Hoppe, P., Crowley, J. N., Ono, S., and Foley, S.: Sulfur isotope fractionation during oxidation of sulfur dioxide: gas-phase oxidation by OH radicals and aqueous oxidation by H₂O₂, O₃ and iron catalysis, *Atmos. Chem. Phys.*, 12, 407–423, doi:10.5194/acp-12-407-2012, 2012.
- Heinold, B., Tegen, I., Esselborn, M., Kandler, K., Knippertz, P., Mueller, D., Schadlitz, A., Tesche, M., Weinzierl, B., Ansmann, A., Althausen, D., Laurent, B., Massling, A., Mueller, T., Petzold, A., Schepanski, K., and Wiedensohler, A.: Regional Saharan dust modelling during the SAMUM 2006 campaign, *Tellus B*, 61, 307–324, doi:10.1111/j.1600-0889.2008.00387.x, 2009.
- Herrmann, H., Ervens, B., Jacobi, H. W., Wolke, R., Nowacki, P., and Zellner, R.: CAPRAM2.3: a chemical aqueous phase radical mechanism for tropospheric chemistry, *J. Atmos. Chem.*, 36, 231–284, 2000.
- Hong, A. P., Bahnemann, D. W., and Hoffmann, M. R.: Cobalt(ii) tetrasulfophthalocyanine on titanium-dioxide. 2. Kinetics and mechanisms of the photocatalytic oxidation of aqueous sulfur-dioxide, *J. Phys. Chem.*, 91, 6245–6251, doi:10.1021/j100308a035, 1987.
- Hoppe, P.: NanoSIMS: a new tool in cosmochemistry, *Appl. Surf. Sci.*, 252, 7102–7106, 2006.
- Janssen, A., Geisler, T., Putnis, C., and Putnis, A.: The mechanism of oxidation and “leaching” of ilmenite during natural and experimental alteration, *Geochim. Cosmochim. Ac.*, 71, A440–A440, 2007.
- Jayne, J. T., Davidovits, P., Worsnop, D. R., Zahniser, M. S., and Kolb, C. E.: Uptake of SO₂(g) by aqueous surfaces as a function of pH – the effect of chemical-reaction at the interface, *J. Phys. Chem.*, 94, 6041–6048, doi:10.1021/j100378a076, 1990.
- Jickells, T. D., An, Z. S., Andersen, K. K., Baker, A. R., Bergametti, G., Brooks, N., Cao, J. J., Boyd, P. W., Duce, R. A., Hunter, K. A., Kawahata, H., Kubilay, N., laRoche, J., Liss, P. S., Mahowald, N., Prospero, J. M., Ridgwell, A. J., Tegen, I., and Torres, R.: Global iron connections between desert dust, ocean biogeochemistry, and climate, *Science*, 308, 67–71, 2005.
- Judeikis, H. S., Stewart, T. B., and Wren, A. G.: Laboratory studies of the heterogeneous reactions of SO₂, *Atmos. Environ.*, 12, 1633–1641, 1978.
- Kaaden, N., Massling, A., Schladitz, A., Mueller, T., Kandler, K., Schuetz, L., Weinzierl, B., Petzold, A., Tesche, M., Leinert, S., Deutscher, C., Ebert, M., Weinbruch, S., and Wiedensohler, A.: State of mixing, shape factor, number size distribution, and hygroscopic growth of the Saharan anthropogenic and mineral dust aerosol at Tinfou, Morocco, *Tellus B*, 61, 51–63, doi:10.1111/j.1600-0889.2008.00388.x, 2009.
- Karge, H. G. and Dalla Lana, I. G.: Infrared studies of SO₂ adsorption on a Claus catalyst by selective poisoning of sites, *J. Phys. Chem.*, 88, 1538–1543, 1984.
- Kim, B. G. and Park, S. U.: Transport and evolution of a winter-time yellow sand observed in Korea, *Atmos. Environ.*, 35, 3191–3201, doi:10.1016/S1352-2310(00)00469-6, 2001.
- Krouse, H. R. and Grinenko, V. A. (Eds.): Stable Isotopes: Natural and Anthropogenic Sulphur in the Environment, Vol. 43, Wiley, Chichester, 1991.
- Krouse, H., Grinenko, L., Grinenko, V., Newman, L., Forrest, J., Nakai, N., Tsuji, Y., Yatsumimi, T., Takeuchi, V., Robinson, B., Stewart, M., Gunatilaka, A., Plumb, L., Smith, J., Buzek, F., Cerny, J., Sramek, J., Menon, A., Iyer, G., Venkatasubramanian, V., Egboka, B., Irogbenachi, M., and Eligwe, C.: Case stud-

- ies and potential applications, in: *Stable Isotopes: Natural and Anthropogenic Sulphur in the Environment*, Chap. 8., edited by: Krouse, H. R. and Grinenko, V. A., John Wiley and Sons, Chichester, 307–416, 1991.
- Kumar, A. and Sarin, M. M.: Aerosol iron solubility in a semi-arid region: temporal trend and impact of anthropogenic sources, *Tellus B – Chem. Phys. Meteorol.*, 62, 125–132, doi:10.1111/j.1600-0889.2009.00448.x, 2010.
- Kumar, A., Sarin, M. M., and Srinivas, B.: Aerosol iron solubility over Bay of Bengal: role of anthropogenic sources and chemical processing, *Mar. Chem.*, 121, 167–175, doi:10.1016/j.marchem.2010.04.005, 2010.
- Lee, C. C. W. and Thiemens, M. H.: The $\delta\text{O-17}$ and $\delta\text{O-18}$ measurements of atmospheric sulfate from a coastal and high alpine region: a mass-independent isotopic anomaly, *J. Geophys. Res.-Atmos.*, 106, 17359–17373, 2001.
- Levin, Z., Ganor, E., and Gladstein, V.: The effects of desert particles coated with sulfate on rain formation in the Eastern Mediterranean, *J. of Appl. Meteorol.*, 35, 1511–1523, 1996.
- Li, L., Chen, Z. M., Zhang, Y. H., Zhu, T., Li, J. L., and Ding, J.: Kinetics and mechanism of heterogeneous oxidation of sulfur dioxide by ozone on surface of calcium carbonate, *Atmos. Chem. Phys.*, 6, 2453–2464, doi:10.5194/acp-6-2453-2006, 2006.
- Li, L., Chen, Z. M., Zhang, Y. H., Zhu, T., Li, S., Li, H. J., Zhu, L. H., and Xu, B. Y.: Heterogeneous oxidation of sulfur dioxide by ozone on the surface of sodium chloride and its mixtures with other components, *J. Geophys. Res.-Atmos.*, 112, D18301, doi:10.1029/2006JD008207, 2007.
- Liao, H. and Seinfeld, J. H.: Global impacts of gas-phase chemistry-aerosol interactions on direct radiative forcing by anthropogenic aerosols and ozone, *J. Geophys. Res.-Atmos.*, 110, D18208, doi:10.1029/2005JD005907, 2005.
- Lin, Y., Sim, M. S., and Ono, S.: Multiple-sulfur isotope effects during photolysis of carbonyl sulfide, *Atmos. Chem. Phys.*, 11, 10283–10292, doi:10.5194/acp-11-10283-2011, 2011.
- Low, M. J. D., Goodsel, A. J., and Takezawa, N.: Reactions of gaseous pollutants with solids. I. Infrared study of the sorption of sulfur dioxide on calcium oxide, *Environ. Sci. Technol.*, 5, 1191–1195, doi:10.1021/es60059a003, 1971.
- Mamane, Y. and Gottlieb, J.: Heterogeneous reactions of minerals with sulfur and nitrogen oxides, *J. Aerosol Sci.*, 20, 303–311, 1989.
- Mariotti, A., Germon, J. C., Hubert, P., Kaiser, P., Letolle, R., Tardieux, A., and Tardieux, P.: Experimental-determination of nitrogen kinetic isotope fractionation – some principles – illustration for the denitrification and nitrification processes, *Plant Soil*, 62, 413–430, 1981.
- Mayer, B., Feger, K. H., Giesemann, A., and Jäger, H. J.: Interpretation of sulfur cycling in two catchments in the Black Forest (Germany) using stable sulfur and oxygen isotope data, *Biogeochemistry*, 30, 31–58, 1995.
- McCabe, J. R., Savarino, J., Alexander, B., Gong, S. L., and Thiemens, M. H.: Isotopic constraints on non-photochemical sulfate production in the Arctic winter, *Geophys. Res. Lett.*, 33, L05810, doi:10.1029/2005GL025164, 2006.
- Morales, C.: The airborne transport of Saharan dust: a review, *Climatic Change*, 9, 219–241, doi:10.1007/BF00140538, 1986.
- Mukai, H., Tanaka, A., Fujii, T., Zeng, Y. Q., Hong, Y. T., Tang, J., Guo, S., Xue, H. S., Sun, Z. L., Zhou, J. T., Xue, D. M., Zhao, J., Zhai, G. H., Gu, J. L., and Zhai, P. Y.: Regional characteristics of sulfur and lead isotope ratios in the atmosphere at several Chinese urban sites, *Environ. Sci. Technol.*, 35, 1064–1071, 2001.
- Ndour, M., Nicolas, M., D’Anna, B., Ka, O., and George, C.: Photoactivity of NO₂ on mineral dusts originating from different locations of the Sahara desert, *Phys. Chem. Chem. Phys.*, 11, 1312–1319, 2009.
- Nicolas, M., Ndour, M., Ka, O., D’Anna, B., and George, C.: Photochemistry of atmospheric dust: ozone decomposition on illuminated titanium dioxide, *Environ. Sci. Technol.*, 43, 7437–7442, 2009.
- Norman, A. L., Barrie, L. A., Toom-Sauntry, D., Sirois, A., Krouse, H. R., Li, S. M., and Sharma, S.: Sources of aerosol sulphate at alert: apportionment using stable isotopes, *J. Geophys. Res.-Atmos.*, 104, 11619–11631, 1999.
- Norris, G., Vedantham, R., Wade, K., Brown, S., Prouty, J., and Foley, C.: EPA Positive Matrix Factorization (PMF) 3.0 Fundamentals and User Guide, US Environmental Protection Agency, Office of Research and Development, Washington, DC, 2008.
- Novak, M., Jackova, I., and Prechova, E.: Temporal trends in the isotope signature of air-borne sulfur in Central Europe, *Environ. Sci. Technol.*, 35, 255–260, 2001.
- Pacchioni, G., Clotet, A., and Ricart, J. M.: A theoretical study of the absorption and reaction of SO₂ at surface and step sites of the MgO(100) surface, *Surf. Sci.*, 315, 337–350, 1994.
- Park, S. H., Song, C. B., Kim, M. C., Kwon, S. B., and Lee, K. W.: Study on size distribution of total aerosol and water-soluble ions during an Asian dust storm event at Jeju Island, Korea, *Environ. Monitor. Assess.*, 93, 157–183, doi:10.1023/B:EMAS.0000016805.04194.56, 2004.
- Pruppacher, H. and Klett, J.: *Microphysics of Clouds and Precipitation*, 2nd edn., Kluwer Academic Publishers, Dordrecht, The Netherlands, 309–360, 1997.
- Putnis, A.: Mineral replacement reactions: from macroscopic observations to microscopic mechanisms, *Mineralogical Magazine*, 66, 689–708, doi:10.1180/0026461026650056, 2002.
- Rani, A., Prasad, D. S. N., Madawat, P. V. S., and Gupta, K. S.: The role of free-fall atmospheric dust in catalyzing autoxidation of aqueous sulfur-dioxide, *Atmos. Environ. A-Gen.*, 26, 667–673, 1992.
- Roithner: Preliminary Information: Hexagonal High-Power UV LED H2A1 UV Series, Roithner Lasertechnik GmbH, Vienna, Austria, available at: http://www.roithner-laser.com/datasheets/led_single/hexagonal/h2a1-uv.pdf, last access: August 2011.
- Rubasinghege, G., Elzey, S., Baltrusaitis, J., Jayaweera, P. M., and Grassian, V. H.: Reactions on atmospheric dust particles: surface photochemistry and size-dependent nanoscale redox chemistry, *J. Phys. Chem. Lett.*, 1, 1729–1737, 2010.
- Rufus, J., Stark, G., Smith, P. L., Pickering, J. C., and Thorne, A. P.: High-resolution photoabsorption cross section measurements of SO₂, 2: 220 to 325 nm at 295 K, *J. Geophys. Res.*, 108, 5011, doi:10.1029/2002JE001931, 2003.
- Saltzman, E. S., Brass, G., and Price, D.: The mechanism of sulfate aerosol formation: chemical and sulfur isotopic evidence, *Geophys. Res. Lett.*, 10, 513–516, 1983.
- Savarino, J., Lee, C. C. W., and Thiemens, M. H.: Laboratory oxygen isotopic study of sulfur (IV) oxidation: origin of the mass-independent oxygen isotopic anomaly in atmospheric sulfates and sulfate mineral deposits on Earth, *J. Geophys. Res.-Atmos.*

- 105, 29079–29088, 2000.
- Sofen, E. D., Alexander, B., and Kunasek, S. A.: The impact of anthropogenic emissions on atmospheric sulfate production pathways, oxidants, and ice core $\Delta^{17}\text{O}(\text{SO}_4^{2-})$, *Atmos. Chem. Phys.*, 11, 3565–3578, doi:10.5194/acp-11-3565-2011, 2011.
- Sullivan, R. C., Guazzotti, S. A., Sodeman, D. A., and Prather, K. A.: Direct observations of the atmospheric processing of Asian mineral dust, *Atmos. Chem. Phys.*, 7, 1213–1236, doi:10.5194/acp-7-1213-2007, 2007.
- Tanaka, T. Y. and Chiba, M.: A numerical study of the contributions of dust source regions to the global dust budget, *Global Planet. Change*, 52, 88–104, doi:10.1016/j.gloplacha.2006.02.002, 2006.
- Tanaka, N., Rye, D. M., Xiao, Y., and Lasaga, A. C.: Use of stable sulfur isotope systematics for evaluating oxidation reaction pathways and in-cloud scavenging of sulfur-dioxide in the atmosphere, *Geophys. Res. Lett.*, 21, 1519–1522, 1994.
- Tilly, J., Lewicki, M., Tomaszewski, Z., and Toczowski, J.: Use of ilmenite decomposition products in a gas desulfurization process, *J. Chem. Technol. Biot.*, 52, 301–310, 1991.
- Torfs, K. M., VanGrieken, R., and Buzek, F.: Use of stable isotope measurements to evaluate the origin of sulfur in gypsum layers on limestone buildings, *Environ. Sci. Technol.*, 31, 2650–2655, 1997.
- Ullerstam, M., Vogt, R., Langer, S., and Ljungstrom, E.: The kinetics and mechanism of SO₂ oxidation by O₃ on mineral dust, *Phys. Chem. Chem. Phys.*, 4, 4694–4699, 2002.
- Ullerstam, M., Johnson, M. S., Vogt, R., and Ljungström, E.: DRIFTS and Knudsen cell study of the heterogeneous reactivity of SO₂ and NO₂ on mineral dust, *Atmos. Chem. Phys.*, 3, 2043–2051, doi:10.5194/acp-3-2043-2003, 2003.
- Umann, B., Arnold, F., Schaal, C., Hanke, M., Uecker, J., Aufmhoff, H., Balkanski, Y., and Dingenen, R. V.: Interaction of mineral dust with gas phase nitric acid and sulfur dioxide during the MINATROC II field campaign: first estimate of the uptake coefficient $\gamma(\text{HNO}_3)$ from atmospheric data, *J. Geophys. Res.-Atmos.*, 110, D22306, doi:10.1029/2005JD005906, 2005.
- Usher, C. R., Al-Hosney, H., Carlos-Cuellar, S., and Grassian, V. H.: A laboratory study of the heterogeneous uptake and oxidation of sulfur dioxide on mineral dust particles, *J. Geophys. Res.-Atmos.*, 107, 4713, doi:10.1029/2002JD002051, 2002.
- Wagner, F., Bortoli, D., Pereira, S., Costa, M., Silva, A., Weinzierl, B., Esselborn, M., Petzold, A., Rasp, K., Heinold, B., and Tegen, I.: Properties of dust aerosol particles transported to Portugal from the Sahara desert, *Tellus B*, 61, 297–306, doi:10.1111/j.1600-0889.2008.00393.x, 2009.
- Winterholler, B.: Sulfur Isotope Analysis of Aerosol Particles by NanoSIMS, Ph.D. thesis, Johannes Gutenberg-Universität, Mainz, Germany, 2007.
- Winterholler, B., Hoppe, P., Andreae, M. O., and Foley, S.: Measurement of sulfur isotope ratios in micrometer-sized samples by NanoSIMS, *Appl. Surf. Sci.*, 252, 7128–7131, 2006.
- Winterholler, B., Hoppe, P., Foley, S., and Andreae, M. O.: Sulfur isotope ratio measurements of individual sulfate particles by NanoSIMS, *Int. J. Mass Spectrom.*, 272, 63–77, 2008.
- Xiao, H., Carmichael, G. R., Durchenwald, J., Thornton, D., and Bandy, A.: Long-range transport of SO_x and dust in East Asia during the PEM B experiment, *J. Geophys. Res.-Atmos.*, 102, 28589–28612, 1997.
- Zender, C., Newman, D., and Tegen, I.: Quantifying mineral dust mass budgets: terminology, constraints, and current estimates, *EOS T. Am. Geophys. Un.*, 85, 509–512, doi:10.1029/2004EO480002, 2004.
- Zhang, X. Y., Zhuang, G. S., Chen, J. M., Wang, Y., Wang, X., An, Z. S., and Zhang, P.: Heterogeneous reactions of sulfur dioxide on typical mineral particles, *J. Phys. Chem. B*, 110, 12588–12596, 2006.
- Zhu, S., Butler, T., Sander, R., Ma, J., and Lawrence, M. G.: Impact of dust on tropospheric chemistry over polluted regions: a case study of the Beijing megacity, *Atmos. Chem. Phys.*, 10, 3855–3873, doi:10.5194/acp-10-3855-2010, 2010.